ANALYSIS OF THE SURFACE MAGNETOPLASMON MODES IN THE SEMICONDUCTOR SLIT WAVEGUIDE AT TERAHERTZ FREQUENCIES

F. M. Kong and K. Li

School of Information Science and Engineering
Shandong University
Jinan 250100, China

H. Huang

School of Electrical Engineering
Beijing Jiaotong University
Beijing 100044, China

B.-I. Wu and J. A. Kong

Research Laboratory of Electronics
Massachusetts Institute of Technology
Cambridge, MA 02139, USA

Abstract—The propagation properties of surface plasmon polaritons (SPP) modes and surface magnetoplasmon polaritons (SMP) modes in a semiconductor slit waveguide are analyzed by the effective dielectric constant approach, and the interaction of the external magnetic field with the dispersion properties and field distributions of SMP modes in the Voigt configuration are emphasized in our analysis. Both the symmetric structure and the asymmetric structure are discussed in details. In contrast to the SPP modes which have one propagation band below the plasmon frequency only, the SMP modes have both the low-frequency propagation band below the plasmon frequency and the high-frequency propagation band above the plasmon frequency. When the external magnetic field increases, the two bands of the SMP modes will separate further in frequency, and the even symmetric distribution of the fundamental mode, which usually associates with the SPP mode, will be destroyed. These results can provide some guidance for the design of the tunable semiconductor waveguide in the terahertz regime.

1. INTRODUCTION

The surface plasmon polaritons (SPP) [1] are essentially light waves that are trapped on the metal surface due to their interaction with the electrons in the metal. The SPP on the metal-dielectric interface has led to a new route in nanophotonics [2, 3]. Enhanced light transmission and light confinement have been found in subwavelength metallic structures [4–9], and in order to guide and confine the SPP in integrated photonic circuits, various plasmonic waveguides have been introduced, such as the V-groove structure [10–12], thin metal strip [13], metal nanoparticle chains [14, 15], metal nanorods [16], and metallic photonic crystals [17]. However, at terahertz (THz) frequencies, the permittivity of the metal is very large, which causes a weak field confinement of SPP to the metal surface and a poor scattering of SPP from the defects in the metal surface [18, 19]. Since the semiconductor has a much lower permittivity than the metal at THz frequencies, it is more suitable for the excitation and confinement of THz SPPs modes. Enhanced transmission at THz frequencies has been observed in hole arrays and groove gratings, which are made from doped silicon or indium antimonide (InSb) [20–25]. In an external magnetic field, due to the cyclotron motion of the electrons in semiconductor, the cyclotron frequency of the doped semiconductor is tunable by changing the magnitude of the external magnetic field. Since an electron has a smaller effective mass in the semiconductor, only a moderate external magnetic field is enough to generate cyclotron frequency in the THz region. The SPP modes under the external magnetic field are also called surface magnetoplasmon polaritons (SMP) modes. A comprehensive review on the dispersion of the SPP and the SMP modes in the semiconductor heterostructure has been presented by Kushwaha [26]. In the past decades, the physics of the SMP modes propagating in the semiconductor-air interface and the thin semiconductor film supported by two semi-infinite dielectrics has been extensively studied [26–33]. However, little work has been done on thin dielectric film bounded by two semi-infinite semiconductors. The semiconductor slit waveguide, similar to the metallic slit waveguide which has exhibited practical subwavelength confinement with moderate propagation loss at optical frequencies [34], has never been explored at THz frequencies.

    In this paper, we present the analysis of the SPP and SMP modes in the semiconductor slit waveguide at THz frequencies by using the effective dielectric constant approach with the dielectric property of the semiconductor being characterized by the gyrodielectric tensor. Both symmetric structure and asymmetric structure are discussed in details,

and the effect of external magnetic field on the dispersion properties and field distributions of the SMP modes is focused on in our work.

2. ANALYSIS METHODOLOGY

The cross section of the semiconductor slit waveguide considered is shown in Figure 1. The dielectric core is bounded by two semiconductors, and two frequency independent dielectrics are used as the cladding and the substrate. The relative dielectric constants of the core, cladding, and substrate are assumed to be ε_{r1}, ε_{rc}, and ε_{rs}. The width and the height of the core are denoted as w and h respectively. When the external magnetic field B_0 is applied in the y-direction and the propagation direction of the guided wave is assumed in the z-direction (Voigt configuration), the relative dielectric constant of the semiconductor can be represented by the gyrodielectric tensor

$$\bar{\bar{\varepsilon}}_{r2} = \begin{bmatrix} \varepsilon_{xx} & 0 & -i\varepsilon_{xz} \\ 0 & \varepsilon_{yy} & 0 \\ i\varepsilon_{zx} & 0 & \varepsilon_{zz} \end{bmatrix} \tag{1}$$

where the elements of this tensor are given by

$$\varepsilon_{xx}(\omega) = \varepsilon_{zz}(\omega) = \varepsilon_\infty \left(1 - \frac{\omega_p^2}{(\omega^2 - \omega_b^2)} \right) \tag{2}$$

$$\varepsilon_{yy}(\omega) = \varepsilon_\infty \left(1 - \frac{\omega_p^2}{\omega^2} \right) \tag{3}$$

$$\varepsilon_{xz}(\omega) = \varepsilon_{zx}(\omega) = \varepsilon_\infty \left(\frac{\omega_p^2 \omega_b}{\omega (\omega^2 - \omega_b^2)} \right) \tag{4}$$

In these equations, ε_∞ is the relative permittivity of the semiconductor at infinite frequency, $\omega_p = \sqrt{Ne^2/m^*\varepsilon_0\varepsilon_\infty}$ is the plasmon frequency, and $\omega_b = eB_0/m^*$ is the cyclotron frequency and is proportional to the static field B_0. Here, N is the electron density, m^* is the effective mass of the free charge carriers in the semiconductor, e is the electronic charge, and ε_0 is the dielectric constant of air. The collision loss in the semiconductor is neglected. For instance, given that InSb has $m^* = 0.015m_0$ (where m_0 is the electron mass in vacuum), $\varepsilon_\infty = 15.68$, and $N \approx 1 \times 10^{22}/m^3$, then $\omega_p = 1.16 \times 10^{13}\,\mathrm{rad/s}$ and $\omega_b/\omega_p \approx B_0$.

In the narrow slit waveguide, the plasmon wave is polarized such that the primary component of magnetic field is tangential to the
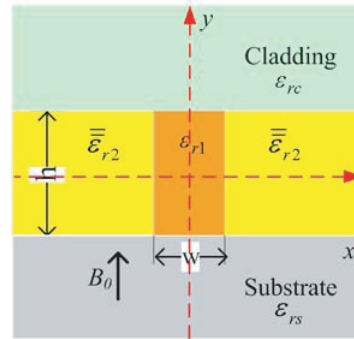
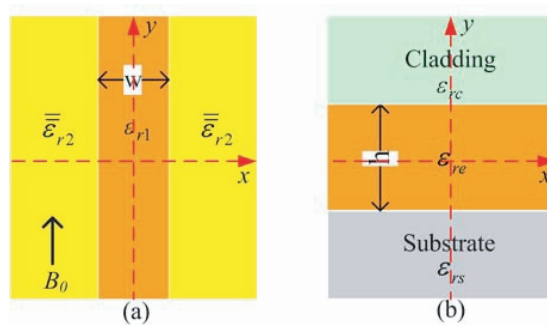**Figure 1.** The cross section of the semiconductor slit waveguide in the Voigt configuration.

Figure 2. The concept of the effective dielectric constant approach, the slit waveguide can be treated as a combination of two coupled one-dimensional slab waveguides in the y and x directions respectively. ε_{re} is the effective relative dielectric constant in the y-direction slab. (a) y-direction slab. (b) x-direction slab.

semiconductor-dielectric interfaces and the electric field is normal to semiconductor-dielectric interfaces, this is to say, E_x and H_y are the primary components in the slit waveguide. According to the effective dielectric constant approach [35, 36], the semiconductor slit waveguide could be treated as a combination of two coupled one-dimensional slab waveguides in the y and x directions respectively (see Figure 2). By deducing the guiding conditions for the TM modes in the y-direction slab and TE modes in the x-direction slab, we can get the dispersion

relation for the SMP modes in the slit waveguide as

$$\left[1 + \left(\frac{\varepsilon_{r1}\gamma_x}{\varepsilon_v k_x}\right)^2 - \left(\frac{\varepsilon_{r1}\varepsilon_{xz}k_z'}{\varepsilon_v \varepsilon_{xx} k_x}\right)^2\right]\tanh(k_x w) = -2\frac{\varepsilon_{r1}\gamma_x}{\varepsilon_v k_x} \qquad (5)$$

$$\left(1 - \frac{\gamma_{cy}\gamma_{sy}}{k_y^2}\right)\tan(k_y h) = \frac{\gamma_{cy} + \gamma_{sy}}{k_y} \qquad (6)$$

where $\varepsilon_v = \varepsilon_{xx} - \varepsilon_{xz}^2/\varepsilon_{xx}$ is the Voigt relative dielectric constant of the semiconductor, $k_z' = k_0^2 \varepsilon_{re}$ and $\varepsilon_{re} = \varepsilon_{r1} + (k_x/k_0)^2$ are propagation constant and the effective relative dielectric constant of the y-direction slab, and the transverse parameters in the two slabs are defined as

$$\gamma_x^2 = k_0^2(\varepsilon_{r1} - \varepsilon_v) + k_x^2 \qquad (7)$$
$$\gamma_{cy}^2 = k_0^2(\varepsilon_{re} - \varepsilon_{rc}) - k_y^2 \qquad (8)$$
$$\gamma_{sy}^2 = k_0^2(\varepsilon_{re} - \varepsilon_{rs}) - k_y^2 \qquad (9)$$

It should be pointed out that the transverse parameters γ_x, γ_{cy}, and γ_{sy}, which indicate the radiation from the slit waveguide, and the condition that $\gamma_x > 0$, $\gamma_{cy} > 0$, and $\gamma_{cs} > 0$ are needed to satisfy the radiation boundary condition at infinity.

To solve k_x and k_y numerically, Eq. (5) can be rewritten as

$$\begin{cases} k_x w = \operatorname{arctanh}(-\rho_{x1}) + \operatorname{arctanh}(-\rho_{x2}) & (p = 1) \\ k_x w = \operatorname{arccoth}(-\rho_{x1}) + \operatorname{arccoth}(-\rho_{x2}) & (p = 2) \end{cases} \qquad (10)$$

and Eq. (6) can be rewritten as

$$k_y h = \arctan(\rho_{cy}) + \arctan(\rho_{sy}) + (q - 1)\pi \quad (q = 1, 2, \dots) \qquad (11)$$

where $\rho_{x1} = \frac{\varepsilon_{r1}}{\varepsilon_v}\left(\frac{\gamma_x}{k_x} + \frac{\varepsilon_{xz}k_z'}{\varepsilon_{xx}k_x}\right)$, $\rho_{x2} = \frac{\varepsilon_{r1}}{\varepsilon_v}\left(\frac{\gamma_x}{k_x} - \frac{\varepsilon_{xz}k_z'}{\varepsilon_{xx}k_x}\right)$, $\rho_{cy} = \frac{\gamma_{cy}}{k_y}$, and $\rho_{sy} = \frac{\gamma_{sy}}{k_y}$.

The hybrid modes associated with the slit waveguides are denoted as E_{pq}^x, where the superscript x denotes the direction of the polarization, and the subscripts $p = 1$ and $p = 2$ correspond to the even and odd symmetries of the field distributions in the x direction in the absence of the external magnetic field, and the subscript q is the number of the peaks in the field along the y direction. In the presence of external magnetic field, the field distribution will be distorted due to the interaction of the external magnetic field. In fact, the E_{2q}^x modes rarely exist in our proposed semiconductor slit waveguide geometry because they are suppressed by the small width and the large ε_∞ of the semiconductor slit waveguide.

Determining the precise mode solution of a semiconductor waveguide involves finding the k_x and k_y in the dispersion relations in Eqs. (10) and (11), the propagation constant k_z can be expressed as

$$k_z = \sqrt{k_0^2 \varepsilon_{r1} + k_x^2 - k_y^2} \qquad (12)$$

3. RESULTS AND DISCUSSION

In this section, the magnetoplasmon dispersion of the semiconductor slit waveguide in the Voigt configuration is studied by using the effective dielectric constant approach, and both symmetric structure ($\varepsilon_{rc} = \varepsilon_{rs}$) and asymmetric structure ($\varepsilon_{rc} \neq \varepsilon_{rs}$) are considered. The dielectric material parameters in the symmetric structure are $\varepsilon_{rc} = \varepsilon_{rs} = 1$ and $\varepsilon_{r1} = 1$, and the dielectric material parameters in the asymmetric structure are $\varepsilon_{rc} = 1$ and $\varepsilon_{rs} = \varepsilon_{r1} = 2.25$, which correspond to the semiconductor slit being embedded in the glass substrate. The parameters $\varepsilon_\infty = 15.68$, $\omega_p = 1.16 \times 10^{13}\,\mathrm{rad/s}$ ($f_p = 1.85\,\mathrm{THz}$) are chosen to model the permittivity of InSb material. The dimensions of the slit waveguide are $w = 0.2\lambda_p$ and $h = 0.4\lambda_p$, where $\lambda_p = 2\pi c/\omega_p$ is the plasmon wavelength.

Before discussing the effect of external magnetic field on the SMP modes, it is worthwhile to study the frequency dependence of the permittivity tensor and the corresponding Voigt relative dielectric constant in the InSb material, Figure 3 shows the results in the cases $\omega_b/\omega_p = 0$ and $\omega_b/\omega_p = 1$. We can see that the frequency dependence curve of Voigt relative dielectric constant in the absence of
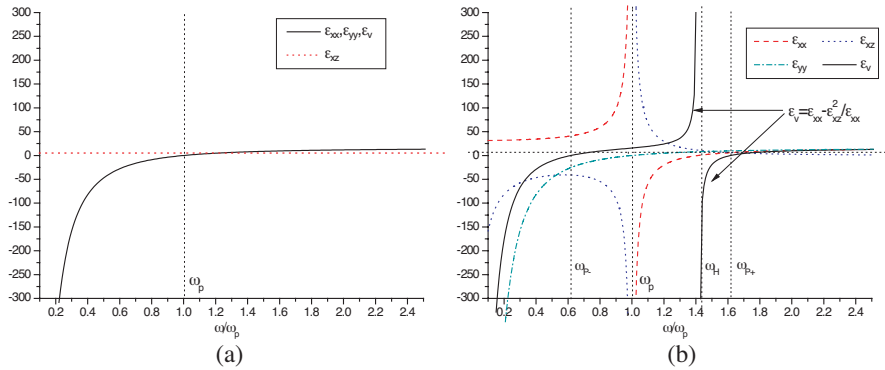

Figure 3. The frequency dependence of the permittivity tensor and the corresponding Voigt dielectric constant for InSb material. (a) $\omega_b/\omega_p = 0$. (b) $\omega_b/\omega_p = 1$.

external magnetic field have one branch and monotonically increases with the frequency. When the external magnetic field is applied, the frequency dependence curve of Voigt relative dielectric constant becomes two branches, which are separated by the hybrid cyclotron plasmon frequency $\omega_H = \sqrt{\omega_b^2 + \omega_p^2}$. The corresponding effective plasmon frequencies for the two branches could then be expressed as

$$\omega_{p\pm} = 0.5 \left(\pm\omega_b + \sqrt{\omega_b^2 + 4\omega_p^2} \right) \tag{13}$$

The Voigt dielectric constant could be negative in the case of $0 < \omega < \omega_{p-}$ and $\omega_H < \omega < \omega_{p+}$. This means that there could be two propagation bands for the SMP modes in the semiconductor slit waveguide when the external magnetic field is applied.
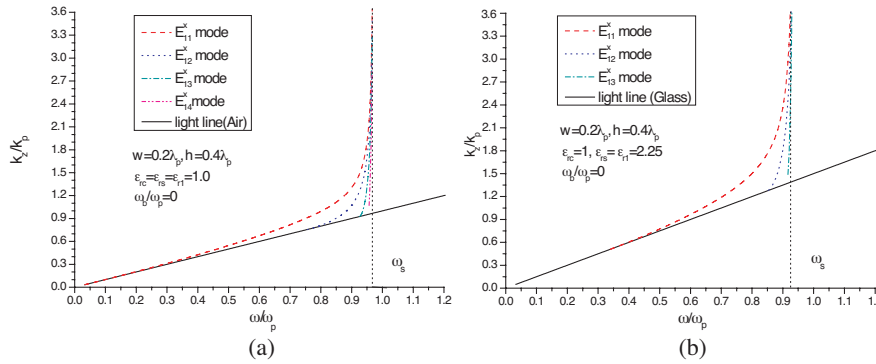

Figure 4. The dispersion of the SPP mode in the InSb slit waveguide. (a) Symmetric structure, $\varepsilon_{rc} = \varepsilon_{rs} = 1$, $\varepsilon_{r1} = 1$. (b) Asymmetric structure, $\varepsilon_{rc} = 1$, $\varepsilon_{rs} = \varepsilon_{r1} = 2.25$.

Next, we focus on the dispersion properties of the SPP modes and the SMP modes in the semiconductor slit waveguide. Figure 4 gives the dispersion properties of the SPP modes in the case of symmetric and asymmetric structures. It is shown that the SPP modes have one propagation band and they are located to the left side of the light line (slow wave region). As the operation frequency increases, all the SPP modes approach the asymptotic frequency ω_s. The asymptotic frequency, which is specified by the solution of $\varepsilon_{xx}(\omega) + \varepsilon_{r1} = 0$, can be expressed as $\omega_s = \omega_p \sqrt{\varepsilon_\infty / (\varepsilon_\infty + \varepsilon_{r1})}$. In the case of the symmetric structure, the fundamental SPP mode E_{11}^x does not have cutoff frequency, whereas the high-order SPP modes have cutoffs at the low-parts of the dispersion curves. In the case of the asymmetric structure, all the SPP modes have cut-off frequencies, which are related
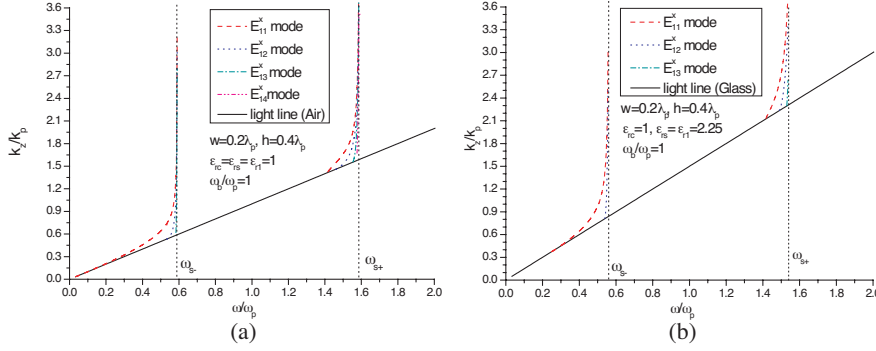
Figure 5. The dispersion of the SMP mode in the InSb slit waveguide in the Voigt configuration. (a) Symmetric structure, $\varepsilon_{rc} = \varepsilon_{rs} = 1$, $\varepsilon_{r1} = 1$. (b) Asymmetric structure, $\varepsilon_{rc} = 1$, $\varepsilon_{rs} = \varepsilon_{r1} = 2.25$.

to the non-symmetry of the cladding and the substrate. Typically, the higher order SPP modes would have higher cut-off frequencies. Due to the interaction of external magnetic field, the dispersion properties of the SMP modes become more complicated than the SPP modes. Figure 5 shows the dispersion properties of the SMP modes in the slit waveguide with $\omega_b/\omega_p = 1$. We can see that all the SMP modes have two propagation bands: the low-frequency band and the high-frequency band which locate below and above the plasmon frequency respectively. The SMP modes in the low-frequency band rise just to the left of the light line and approach the asymptotic frequency ω_{s-}, while the SMP modes in the high-frequency band start from the hybrid cyclotron plasmon frequency ω_H and approach the asymptotic frequency ω_{s+}. The asymptotic frequency for SMP modes, which is specified by the solution of $\varepsilon_{xx}(\omega) + \varepsilon_{xz}(\omega) + \varepsilon_{r1} = 0$, can be expressed as

$$\omega_{s\pm} = 0.5 \left(\pm \omega_b + \sqrt{\omega_b^2 + 4\varepsilon_\infty \omega_p^2/(\varepsilon_\infty + \varepsilon_{r1})} \right) \qquad (14)$$

It should be noted that the two asymptotic SMP modes are separated by $|\omega_b|$. The SMP modes in the low-frequency band have the similar dispersion properties to the SPP modes. In the case of asymmetric structure, all the SMP modes have cut-off frequencies also, especially for the SMP modes in the low-frequency band.

In order to elucidate the effect of the external magnetic field on the dispersion properties of the SMP modes, the band map of the E_{11}^x mode in the slit waveguide is given in Figure 6 with ω_b/ω_p in the range of 0–2 Tesla. From Figure 6, we can see that the E_{11}^x mode has one

propagation band when no external magnetic field is applied, but has two propagation bands when the external magnetic field is greater than the critical value for the emergence of the high-frequency SMP modes. The critical cyclotron frequency, which could be specified by the condition $\omega_{s+} > \omega_H$, can be expressed as $\omega_{bc} = \omega_p/\sqrt{(\varepsilon_\infty/\varepsilon_{r1})^2 - 1}$. This means that the external magnetic field B_0 must be at least 0.064 Tesla and 0.145 Tesla to meet the condition for the high-frequency band emerging in our proposed symmetric and asymmetric structures, separately. As the external magnetic field increases, the propagation band of the low-frequency modes moves to lower frequency, whereas the propagation band of the high-frequency modes shifts to higher frequency. The effect can be explained by the fact that the effective plasmon frequency ω_{p-} decreases and ω_{p+} increases when the external magnetic field increases.
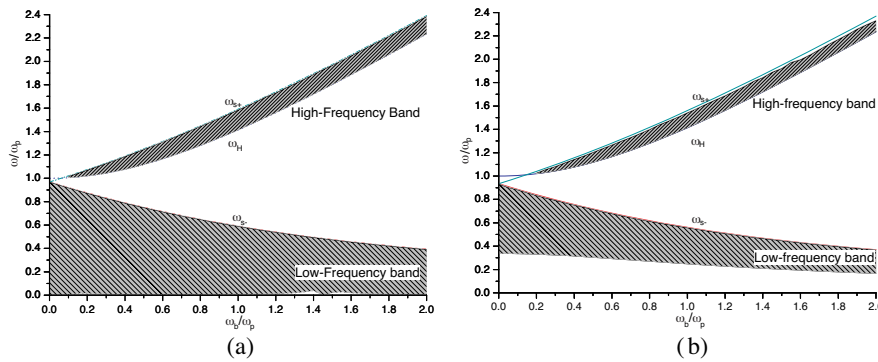

Figure 6. The band map of the SMP E_{11}^x mode in the InSb slit waveguide in the Voigt configuration. (a) Symmetric structure, $\varepsilon_{rc} = \varepsilon_{rs} = 1$, $\varepsilon_{r1} = 1$. (b) Asymmetric structure, $\varepsilon_{rc} = 1$, $\varepsilon_{rs} = \varepsilon_{r1} = 2.25$.

Now, we turn our attention to the field distributions of the SPP modes and SMP modes. The normalized H_y distribution of the SPP E_{11}^x mode in the slit waveguide is illustrated in Figure 7. It is shown that the H_y distribution of the SPP E_{11}^x mode in the symmetric structure is symmetric in both width direction and height direction, while the H_y distribution of the SPP E_{11}^x mode in the asymmetric structure is symmetric only in the width direction. We can also observe that the evanescent fields of the SPP E_{11}^x mode decay faster into the semiconductor than in the cladding and the substrate. As the operation frequency increases, there is more energy confined in the core of the slit waveguide. When the external magnetic field is applied, the field profiles of the SMP modes will be affected. Figure 8 gives the normalized H_y distribution of the SMP E_{11}^x mode in the case of

$\omega_b/\omega_p = 1$. It is shown that the symmetric distribution of the magnetic field H_y of the SMP E_{11}^x mode is distorted due to the interaction of the external magnetic field. When the operation frequency increases, there is more energy confined in the right semiconductor-dielectric interface when the SMP E_{11}^x mode is in the low-frequency band, while in the left semiconductor-dielectric interface in the high-frequency band.
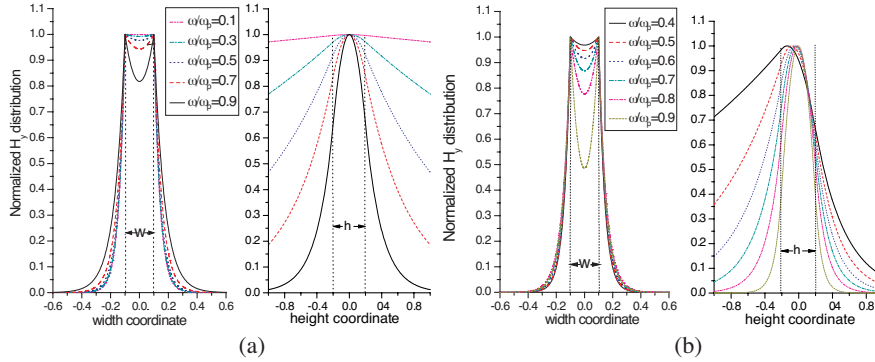

Figure 7. The normalized H_y distribution of the SPP E_{11}^x mode in the InSb slit waveguide. (a) Symmetric structure, $\varepsilon_{rc} = \varepsilon_{rs} = 1$, $\varepsilon_{r1} = 1$. (b) Asymmetric structure, $\varepsilon_{rc} = 1$, $\varepsilon_{rs} = \varepsilon_{r1} = 2.25$.
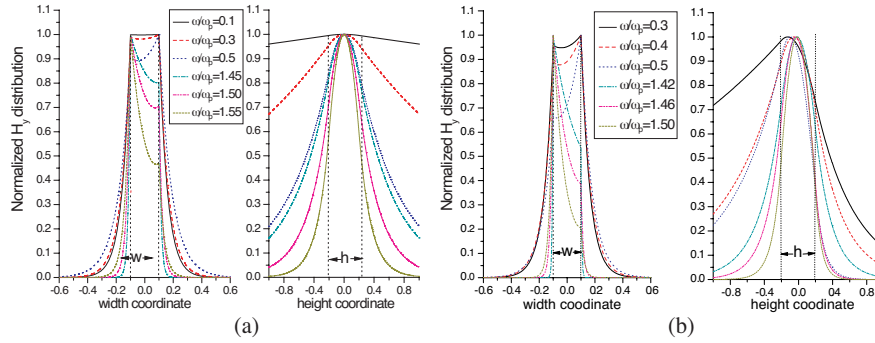

Figure 8. The normalized H_y distribution of the SMP E_{11}^x mode in the InSb slit waveguide in the Voigt configuration. (a) Symmetric structure, $\varepsilon_{rc} = \varepsilon_{rs} = 1$, $\varepsilon_{r1} = 1$. (b) Asymmetric structure, $\varepsilon_{rc} = 1$, $\varepsilon_{rs} = \varepsilon_{r1} = 2.25$.

4. SUMMARY

We present a detail study on the properties of the SPP and SMP modes in the semiconductor slit waveguide by using the effective dielectric constant approach, especially emphasis on the interaction of external magnetic field with the dispersion properties and the field profiles of the SMP modes in the semiconductor slit waveguide in the Voigt configuration, and both the symmetric and asymmetric structures are discussed in details. In comparison with the single propagation band in the SPP modes, the SMP modes have two propagation bands: the low-frequency band and the high-frequency band, which will shift towards lower frequency and higher frequency respectively when the external magnetic field increases. In the presence of the external magnetic field, the symmetry of field distribution, which usually associated with the SPP fundamental mode, is distorted by the interaction of the external magnetic field. When the operation frequency increases, for the SMP mode in the low-frequency band, there is more energy confined in the right semiconductor-dielectric interface, while for the modes in the high-frequency band it confined in left semiconductor-dielectric interface. These results can provide some guidance for the design of the tunable semiconductor waveguide in THz frequencies.

ACKNOWLEDGMENT

REFERENCES

1. Zayats, A. V., I. I. Smolyaninov, and A. A. Maradudin, "Nano-optics of surface plasmon polaritons," *Phys. Rep.*, Vol. 408, No. 3–4, 131–314, 2005.
2. Prasad, P. N., *Nanophotonics*, Wiley-Interscience, New Jersey, 2004.
3. Ozbay, E., "Plasmonics: Merging photonics and electronics at manoscale dimensions," *Science*, Vol. 311, No. 5758, 189–193, 2006.

4. Chang, C. K., D. Z. Lin, C. S. Yeh, et al., "Experimental analysis of surface plasmon behavior in metallic circular slits," *Appl. Phys. Lett.*, Vol. 90, No. 6, 2007.

5. Gordon, R., L. K. S. Kumar, and A. G. Brolo, "Resonant light transmission through a nanohole in a metal film," *IEEE Trans. on Nanotechnology*, Vol. 5, No. 3, 291–294, 2006.

6. Lin, L., R. J. Reeves, and R. J. Blaikie, "Surface-plasmon-enhanced light transmission through planar metallic films," *Phys. Rev. B*, Vol. 74, No. 15, 2006.

7. Xiao, S., N. A. Mortensen, and M. Qiu, "Enhanced transmission through arrays of subwavelength holes in gold films coated by a finite dielectric layer," Arxiv preprint *Physics: 0703092*, 2007.

8. Kong, F., B. I. Wu, H. Chen, et al., "Surface plasmon mode analysis of nanoscale metallic rectangular waveguide," *Opt. Exp.*, Vol. 15, No. 19, 12331–12337, 2007.

9. Lin, L., R. J. Blaikie, and R. J. Reeves, "Surface-plasmon-enhanced optical transmission through planar metal films," *Journal of Electromagnetic Waves and Applications*, Vol. 19, 1721–1728, 2005.

10. Seidel, J., "Surface plasmon transmission across narrow grooves in thin silver films," *Appl. Phys. Lett.*, Vol. 82, No. 9, 1368, 2003.

11. Pile, D. F. P. and D. K. Gramotnev, "Channel plasmon-polariton in a triangular groove on a metal surface," *Opt. Lett.*, Vol. 29, No. 10, 1069–1071, 2004.

12. Bozhevolnyi, S. I., V. S. Volkov, E. Devaux, et al., "Channel plasmon-polariton guiding by subwavelength metal grooves," *Phys. Rev. Lett.*, Vol. 95, No. 4, 46802, 2005.

13. Breukelaar, I., R. Charbonneau, and P. Berini, "Long-range surface plasmon-polariton mode cutoff and radiation," *Appl. Phys. Lett.*, Vol. 88, No. 5, 051119, 2006.

14. Maier, S. A., "Observation of coupled plasmon-polariton modes in Au nanoparticle chain waveguides of different lengths: Estimation of waveguide loss," *Appl. Phys. Lett.*, Vol. 81, No. 9, 1714, 2002.

15. Liaw, J. W., M. K. Kuo, and C. N. Liao, "Plasmon resonances of spherical and ellipsoidal nanoparticles," *Journal of Electromagnetic Waves and Applications*, Vol. 19, No. 13, 1787–1794, 2005.

16. Imura, K., T. Nagahara, and H. Okamoto, "Near-field optical imaging of plasmon modes in gold nanorods," *J. Chem. Phys.*, Vol. 122, No. 15, 154701, 2005.

17. El-Kady, I., M. M. Sigalas, R. Biswas, et al., "Metallic photonic

crystals at optical wavelengths," *Phys. Rev. B*, Vol. 62, No. 23, 15299–15302, 2000.

18. Xu, C., X. Hu, Y. Li, et al., "Semiconductor-based tunable photonic crystals by means of an external magnetic field," *Phys. Rev. B*, Vol. 68, No. 19, 193201, 2003.

19. Lan, Y. C., Y. C. Chang, and P. H. Lee, "Manipulation of tunneling frequencies using magnetic fields for resonant tunneling effects of surface plasmons," *Appl. Phys. Lett.*, Vol. 90, 171114, 2007.

20. Rivas, J. G., C. Janke, P. H. Bolivar, et al., "Transmission of THz radiation through InSb gratings of subwavelength apertures," *Appl. Opt.*, Vol. 4, S83, 2002.

21. Rivas, J. G., C. Schotsch, P. H. Bolivar, et al., "Enhanced transmission of THz radiation through subwavelength holes," *Phys. Rev. B*, Vol. 68, 201306, 2003.

22. Kuttge, M., H. Kurz, J. G. Rivas, et al., "Analysis of the propagation of terahertz surface plasmon polaritons on semiconductor groove gratings," *J. Appl. Phys.*, Vol. 101, 023707, 2007.

23. Rivas, J. G., C. Janke, P. Bolivar, et al., "Transmission of THz radiation through InSb gratings of subwavelength apertures," *Opt. Exp.*, Vol. 13, No. 3, 847–859, 2005.

24. Rivas, J. G., M. Kuttge, P. H. Bolivar, et al., "Propagation of surface plasmon polaritons on semiconductor gratings," *Phys. Rev. Lett.*, Vol. 93, No. 25, 256804, 2004.

25. Kuttge, M., H. Kurz, J. G. Rivas, et al., "Analysis of the propagation of terahertz surface plasmon polaritons on semiconductor groove gratings," *JPN. J. Appl. Phys.*, Vol. 101, 023707, 2007.

26. Kushwaha, M. S., "Plasmons and magnetoplasmons in semiconductor heterostructures," *Surf. Sci. Rep.*, Vol. 41, No. 1–8, 1–416, 2001.

27. Eroglu, A. and J. K. Lee, "Dyadic Green's functions for an electrically gyrotropic medium," *Progress In Electromagnetics Research*, PIER 58, 223–241, 2006.

28. Elmzughi, F. G. and D. R. Tilley, "Surface and guided-wave polariton modes of magnetoplasma films in the Voigt geometry," *J. Phys.-Condens. Mat.*, Vol. 6, No. 23, 4233–4246, 1994.

29. Sarid, D., "Enhanced surface-magnetoplasma interactions in a semiconductor," *Phys. Rev. B*, Vol. 29, No. 4, 2344–2346, 1984.

30. Kushwaha, M. S. and P. Halevi, "Magnetoplasmons in thin films in the Voigt configuration," *Phys. Rev. B*, Vol. 36, No. 11, 5960–5967, 1987.

31. Kushwaha, M. S. and P. Halevi, "Magnetoplasmons in thin films in the perpendicular configuration," *Phys. Rev. B*, Vol. 38, No. 17, 12428–12435, 1988.

32. Huang, H., Y. Fan, B. I. Wu, et al., "Surface modes at the interfaces between isotropic media and uniaxial plasma," *Progress In Electromagnetics Research*, PIER 76, 1–14, 2007.

33. Eroglu, A. and J. K. Lee, "Wave propagation and dispersion characteristics for a nonreciprocal electrically gyrotropic medium," *Progress In Electromagnetics Research*, PIER 62, 237–260, 2006.

34. Kong, F. M., K. Li, B. I. Wu, et al., "Propagation properties of the SPP modes in nanoscale narrow metallic gap, channel, and hole geometries," *Progress In Electromagnetics Research*, PIER 76, 449–466, 2007.

35. Rozzi, T. and M. Mongiardo, *Open Electromagnetic Waveguides*, Institution of Electrical Engineers, London, 1997

36. Marcatili, E. A. J., "Dielectric rectangular waveguide and directional coupler for integrated optics," *The Bell System Technical Journal*, Vol. 48, No. 7, 2071–2102, 1969